Hindawi
International Journal of RF and Microwave Computer-Aided Engineering
Volume 2023, Article ID 6369944, 12 pages
https://doi.org/10.1155/2023/6369944

Research Article

A Highly Transparent Flexible Antenna Based on Liquid Metal Mesh Film

Peng Qin,[1,2] Qianyu Wang,[1,2] Pan Zhang,[1,2] Guanlong Huang,[3] Qian Li,[1,2] Bingxin Liu,[1,2] Lei Li,[1,2] Lin Gui,[1,2] Jing Liu,[1,2] and Zhongshan Deng[1,2]

[1]*Technical Institute of Physics and Chemistry, Chinese Academy of Sciences, Beijing 100190, China*
[2]*School of Future Technology, University of Chinese Academy of Sciences, Beijing 100049, China*
[3]*School of AI—Guangdong & Taiwan, Foshan University, Foshan 528225, China*

Correspondence should be addressed to Zhongshan Deng; zsdeng@mail.ipc.ac.cn

Received 11 November 2022; Revised 6 March 2023; Accepted 10 April 2023; Published 26 April 2023

Academic Editor: Chow-Yen-Desmond Sim

In this paper, a convenient process for the fabrication of flexible liquid metal mesh films (LMMF) is proposed first. Then, the light transmittance and square resistance characteristics of LMMF are studied theoretically and experimentally. The light transmittance of the LMMF can reach 85% when the line width and spacing are 50 μm and 1000 μm, respectively. Furthermore, as an example of LMMF, a coplanar waveguide loop antenna is designed and fabricated that contains an LMMF with a line width of 50 μm and a line spacing of 500 μm. The measured square resistance and transmittance for the LMMF are 0.0456 Ω/sq and 72%, respectively. The measured peak gain of the antenna is 3.38 dBi while the average efficiency is 61%. The antenna's working frequency covers most of the S-band, C-band, and X-band, as well as multiple channels of fifth generation (5G) communication. Therefore, the antenna can be used in fields such as radar and mobile communication. Uniquely, the fabricated antenna performs well in terms of light transmission, conductivity, and flexibility. In particular, it remains stable in stretching and bending deformation. As a highly light-transmissive stretchable flexible antenna, the antenna is equipped with various functions such as concealability, conformability, and reconfigurability. This LMMF-based antenna has good prospects for applications in the fields of flexible electronics and transparent electronics.

1. Introduction

With the gradual rise of fifth generation (5G) wireless technology and the Internet of Things, the research and application of optically transparent antennas have received increasing attention in recent years [1–7]. Optically transparent antennas can be attached to the surface of various transparent substrates in applications that are not easily recognized by the naked eye and can play an important role in concealment and aesthetics [1–7]. Therefore, transparent antennas have been installed on vehicle glass, solar panels of satellites, architectural glass, etc. However, with the increasing complexity of application scenarios, simple transparent antennas have been difficult to meet the usage requirements. For example, when antennas are used on objects with complex shapes, they often also need to have conformal capabilities [8–10]. A better solution is to make the antenna itself flexible. Furthermore, multifunctional antennas like bandwidth-enhanced and reconfigurable antennas [11–15] are in keen demand. In particular, in wearable electronic [16], antennas are expected to be stretchable in the presence of motion and deformation. Therefore, flexible stretchable antennas with high transmission have good prospects for development.

The substrate material and the conductive material of the antenna are key factors for the light transmission, flexibility, and stretchability of the antenna. So far, a variety of transparent substrates have been used to manufacture transparent antennas, including glass [1, 3, 12, 13, 17–19], polyimide (PI) [2], polydimethylsiloxane (PDMS) [5], plexiglass [6], polyethylene terephthalate (PET) [7, 20, 21], polyvinyl

chloride (PVC), and Ecoflex™. These materials are different in various aspects, such as dielectric properties, hardness, brittleness, and light transmission. For example, glass has high light transmittance and is difficult to stretch and bend once formed. Ecoflex™ is very flexible but less light transmitting. Among them, PDMS is increasingly used by researchers because of its good flexibility, stretchability, and light transmission, as well as its ease of molding [5].

Conductive materials are also indispensable as the key element for transparent antennas. Most existing studies use transparent conductive oxides as conductor materials, such as indium tin oxide (ITO) [1, 12, 13] and fluorine-doped tin oxide (FTO) [22, 23]. However, conductive oxides have problems of large square resistance and high brittleness. Researchers have tried to sandwich a conductor layer in the middle of the transparent conductive oxide [2, 3, 17–21] or coat it with gold on its surface [1] to improve the conductivity of the transparent antenna. However, due to the limited thickness of the added conductor layer, the conductivity improvement is also limited, and the brittleness problem remains unavoidable. In fact, in order to improve the conductivity, the direct fabrication of the antenna radiation unit with metallic conductors is the best strategy. In this case, considering the light transmittance, the metal must be made into a metal mesh with light leakage.

Elmobarak Elobaid et al. used a transparent conductive fabric tissue on a polydimethylsiloxane (PDMS) substrate to obtain a flexible and transparent ultrawideband (UWB) antenna. The fabric tissue measured resistivity was 0.089 Ω/sq with a thickness of 0.057 mm, which consisted of woven meshed polyester fibers and coated with nickel/zinc-blackened copper. The measured optical transmittance exceeded 70% across the entire visible spectrum (from 400 to 800 nm). This work had high transmittance because the PDMS was used as the substrate material, but the antenna could only be properly bent and not stretched because its conductive element was made of woven meshed polyester fibers that were coated with nickel/zinc-blackened copper. Tung and Jung, Hong et al., Kim et al., and Hong et al. published a series of works on transparent antennas [2, 6, 7, 17]. In their 2019 study, they fabricated a high-light transmission antenna based on copper mesh [7]. The antenna had a light transmission rate of over 70% and a low sheet resistance of 0.04 Ω/sq. The average efficiency of the transparent patch antenna was 83.8% when using capacitive feed. However, the solid metal mesh has certain limitations in flexibility, stretchability, and bendability. Therefore, it is worth investigating stretchable light-transmitting antennas with new materials and processes.

Liquid metals (LM) refer to metals or alloys that are liquid at room temperature [24]. Due to their good conductivity, fluidity, and modified printability, they are used in the design and fabrication of coaxial phase shifters [25], waveguides [26], antennas, etc. [27–29]. In 2018, Pan et al. [30] proposed a method to make transparent and stretchable circuits by first plating the copper/chromium layer and then adhering the LM to the copper/chromium layer. In 2021, Dejace et al. [31] also manufactured a transparent stretchable circuit by first plating a layer of gold and then attaching gallium. Compared to pure solid metal, the LM film has better tensile performance. However, the processes of these two studies are very complex, and there is still a solid metal layer that is prone to wrinkling during stretching.

This paper presents a simple strategy to fabricate LMMF, which is used to fabricate antennas with excellent performance in terms of flexibility, conductivity, and optical transmission. First, the transmittance and square resistance characteristics of LMMF are investigated theoretically and experimentally. Then, to validate the design concept, a prototype of a coplanar waveguide loop antenna is manufactured. Finally, the performance of the coplanar waveguide loop antenna is simulated and measured, including the reflection coefficient and gain. The antennas manufactured in this paper can be used in radar and mobile communication fields, and the new materials and processes used can provide a reference for the research of transparent and wearable electronics. Detailed discussions of LMMF and the LMMF-based antenna are presented below.

2. Liquid Metal Mesh Films

2.1. The Configuration of LMMF. Figure 1 shows the configuration of a square LMMF. The black part of the figure was the liquid metal mesh made of gallium-indium eutectic alloy (EGaIn, the gallium-indium mass ratio is 75.5 : 24.5), and the blue substrate used for illustration was made of PDMS (Sylgard 184, Dow Corning). EGaIn was encapsulated in PDMS to prevent leakage and oxidation. According to the notes in Figure 1, the line width is w, and the line spacing is s. The thickness of EGaIn is H, the thickness of the substrate that covers EGaIn is T_1, and the thickness of the underlying substrate is T_2. The total lengths of the LM mesh and film are W and L, respectively.

2.2. The Fabrication Process of LMMF. Figure 2 shows the process flow for the fabrication of LMMF. The first step was to use soft lithography to make a mold with a convex grid on the surface of a silicon wafer. Next, the liquid PDMS base and the curing agent were weighed according to the mass ratio of 10 : 1, then mixed. The mixture was stirred manually for 10 minutes and kept under vacuum for 30 minutes to remove air bubbles from the mixture. Then, an appropriate amount of PDMS was poured into the mold placed in a Petri dish and baked at 75°C for 2.5 hours to solidify the liquid PDMS completely. Subsequently, film A with a concave grid was formed and removed from the silicon wafer. Film B with flat surfaces was produced in a similar way, and a small hole was punched in the appropriate position of one corner of film B. In the following process, a plasma bonder (YZD08-2C, Tangshan Yanzhao Technology, China) was used to treat the surface of film A with a grid structure and the surface of one side of film B, and then, the two surfaces were bonded to obtain film C with grid flow channels. Film C was heated on a heating plate at 90°C for 10 minutes to increase the bonding effect. After that, an EGaIn droplet was dropped on the surface of the small hole in film C, and film C with the EGaIn droplet was placed in a vacuum chamber. A high vacuum of 10^{-4} Pa was obtained in the vacuum chamber by a molecular pump. When the pressure in the vacuum chamber was restored to atmospheric pressure, EGaIn was filled into film C, thus

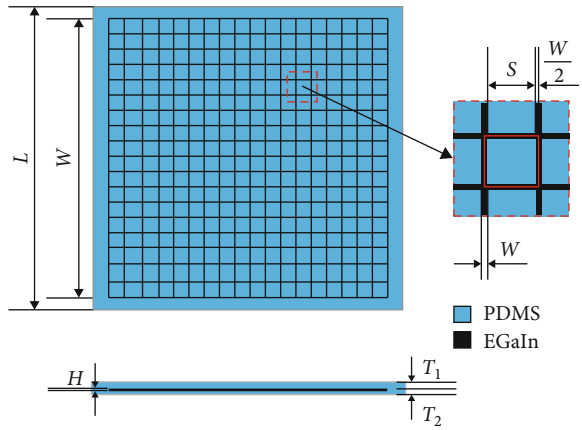

Figure 1: Schematic diagram of the LMMF.

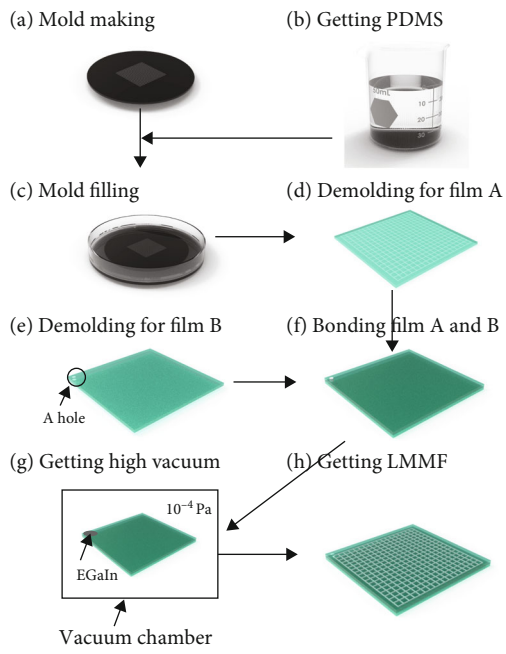

Figure 2: Process flow chart for making LMMF. (a) A mold was made on the silicon wafer. (b) Obtaining liquid PDMS without bubbles. (c) The specified volume of liquid PDMS was poured into the mold. (d) After the PDMS was cured, film A with grid channels on its surface was removed from the mold. (e) Using a similar process, film B was made with flat surfaces, and a small hole was punched in the appropriate position of one corner of film B. (f) Film A and film B were bonded to obtain film C with grid flow channels inside the double-layer film. (g) A droplet of EGaIn was dropped on the surface of the small hole in film C, which was then placed in a vacuum chamber later, and the vacuum degree in the vacuum chamber was reduced to 10^{-4} Pa. (h) When the pressure in the vacuum chamber was restored to atmospheric pressure, EGaIn was filled into film C, thus obtaining the LMMF.

obtaining LMMF. Finally, excess EGaIn was removed around the small hole and sealed with an appropriate amount of glue.

2.3. The Transmittance of LMMF. Ignoring half the line width of LM lines at the edges of the LMMF, it (as shown in Figure 1)

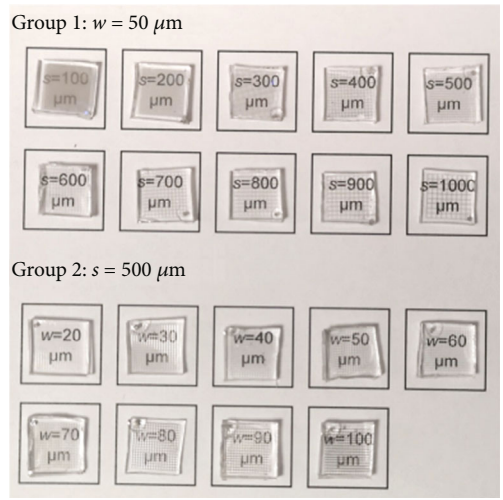

Figure 3: LMMF with different line widths and line spacings.

can be regarded as a seamless splicing of many small grids with a side length of $s + w$. Taking a small grid as the object of investigation, there is a nonmetallized area with side length s at the center of the grid, and the edge of this unit is a square boundary of width $w/2$. The area ratio of the nonmetallized area to the unit can be calculated as

$$\alpha = \frac{s^2}{(s+w)^2}. \tag{1}$$

If the transmittance of the PDMS was A, then the transmittance of the LMMF can be expressed as

$$T(s,w) = A \times \left(\frac{s}{s+w}\right)^2, \tag{2}$$

where s and w are independent and uncorrelated. The derivatives of $T(s, w)$ with respect to s and w can be obtained, respectively, as

$$\begin{aligned} \frac{dT}{ds} &= \frac{2sw}{(s+w)^3}, \\ \frac{dT}{dw} &= \frac{-2s^2}{(s+w)^3}. \end{aligned} \tag{3}$$

Since both s and w are greater than zero, we can get the following.

$$\begin{aligned} \frac{dT}{ds} &> 0, \\ \frac{dT}{dw} &< 0. \end{aligned} \tag{4}$$

According to the monotonicity principle, $T(s, w)$ increases with s and decreases with w.

As shown in Figure 3, there are two groups of LMMF samples with different line width w and line spacing s. The first group shows samples with the line spacing s gradually

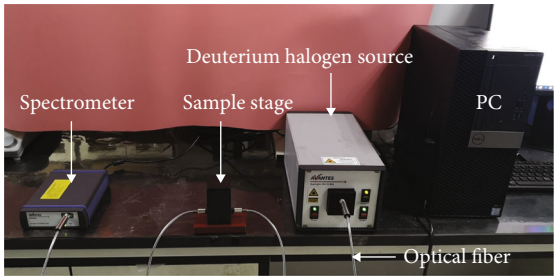

Figure 4: Transmittance measurement system.

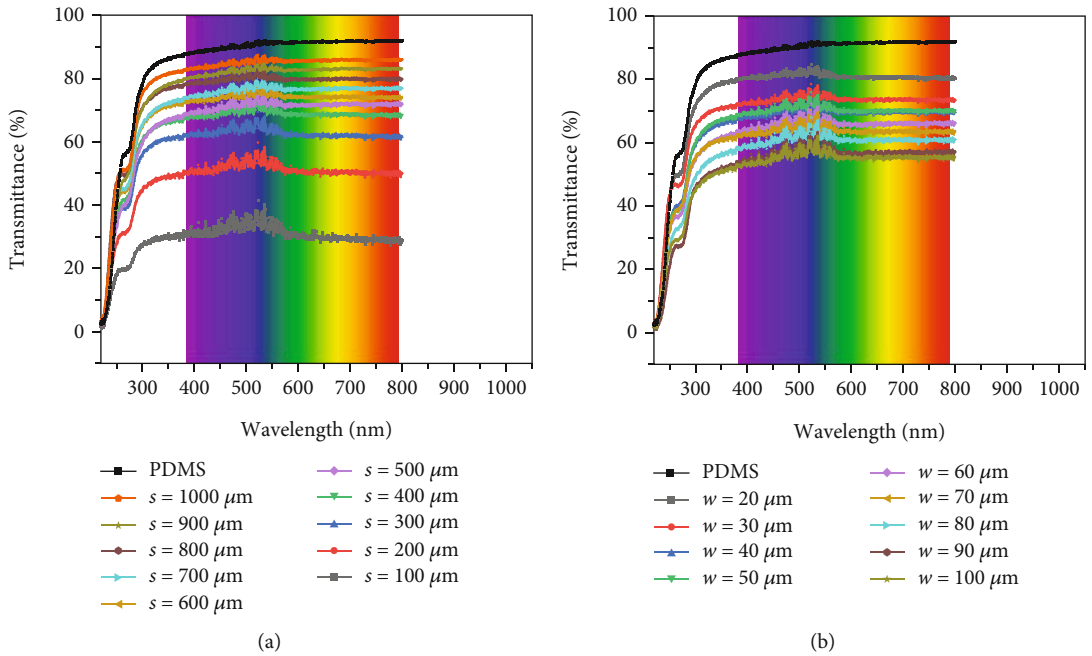

Figure 5: The measured results for the transmittance of LMMF. (a) The transmittance of LMMF with different line spacings s (line width $w = 50\,\mu$m). (b) The transmittance of LMMF with different line width w (line spacing $s = 500\,\mu$m).

increasing from 100 μm to 1000 μm, while the line width w remains 50 μm. The second group shows samples where the line width w gradually increases from 20 μm to 100 μm, while the line spacing s is kept at 500 μm. In the second group, EGaIn failed to be injected into the flow channels when the sample line width was 10 μm. A larger pressure difference may be required to obtain narrower line widths than 20 μm by the preparation process described herein.

Figure 4 shows the components of the light transmittance measurement system (spectrometer: AvaSpec-ULS2048CL-EVO; light source: AvaLight-DH-S-BAL, both produced by Avantes, Netherlands) for measuring the transmittance of LMMF in the visible light range.

Figure 5 shows the results of light transmittance measurements, in which Figure 5(a) demonstrates the measurement results of group 1 shown in Figure 3. It indicates that the transmittance (average value in the visible light range) increases from 31% to 85% when the line spacing s gradually increases from 100 μm to 1000 μm. As shown in Figure 5(b), the average transmittance for group 2 shown in Figure 3 decreases from 81% to 55% when the line width w is gradually increased from 20 μm to 100 μm. Furthermore, the curves in Figure 5(b) are more concentrated, and the average transmittance is greater than 50%. It indicates that the effect of line width w on transmittance is smaller than that of line distance s in the two sets of data selected for line width w and line distance s. Moreover, Figure 5 also shows the trend of light transmittance, which is consistent with the theoretical derivation results. When the line width w and the line spacing s are 50 μm and 500 μm, respectively, the average light transmittance is 72%. The average transmittance of PDMS without LM meshes is 91%. The data is taken into (2) to obtain the calculated transmittance of the film for different line widths and line spacings, as shown in Figure 6.

Figures 6(a) and 6(b) show the calculated transmittance of the films for different line width w and line spacing s. The average value of the transmittance over the entire visible range is then used as the transmittance of the film. Then, the average

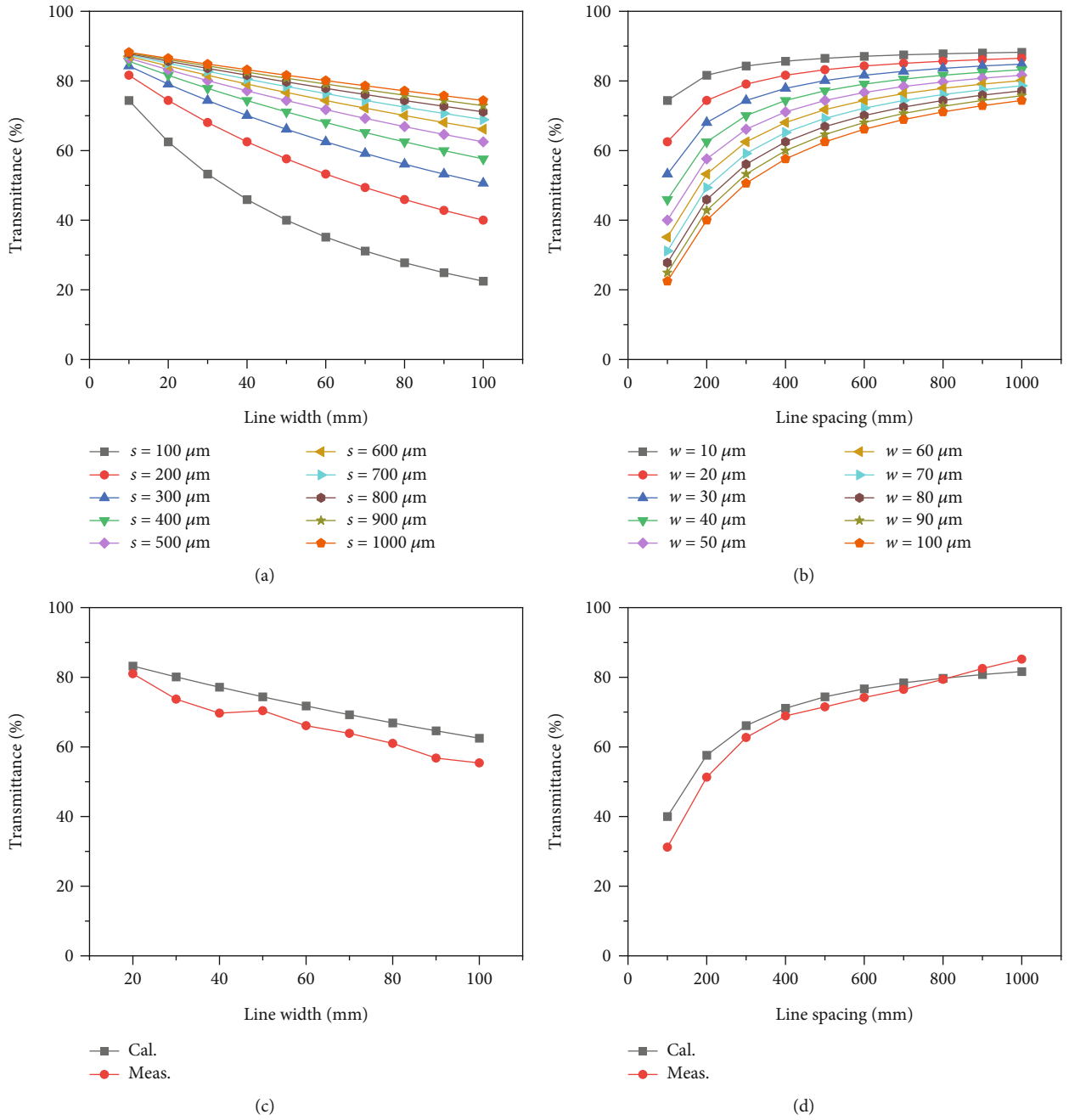

Figure 6: Calculated and simulated light transmittance of the LMMF. (a) Calculated transmittance of the film under different line width w. (b) Calculated transmittance of the film at different line spacing s. (c) The measured and calculated light transmittances of the films at different width w (line spacing $s = 500\ \mu$m). (d) The measured and calculated light transmittances of the films at different line spacing s (line width $w = 50\ \mu$m).

value of the transmittance over the entire visible range is used as the measured transmittance, and a comparison graph of the calculated and measured transmittances of the two sets of samples can be obtained. From Figures 6(c) and 6(d), it is known that in most cases, the measured transmittance is slightly lower than the calculated value, but the trend is quite consistent. The errors may come from the dimensional errors of the fabricated samples.

2.4. The Square Resistance of LMMF. To thoroughly understand the series-parallel problem of a bounded $N \times M$ small resistance involved in LMMF, it is necessary to theoretically calculate the square resistance R of LMMF. In this case, the simplified physical model of the square resistance could be expressed as follows [32].

$$R = \rho \frac{s + w}{wH}, \tag{5}$$

where ρ represents the electrical resistivity of LM and s, w, and H are the line spacing, the line width, and the line height, respectively.

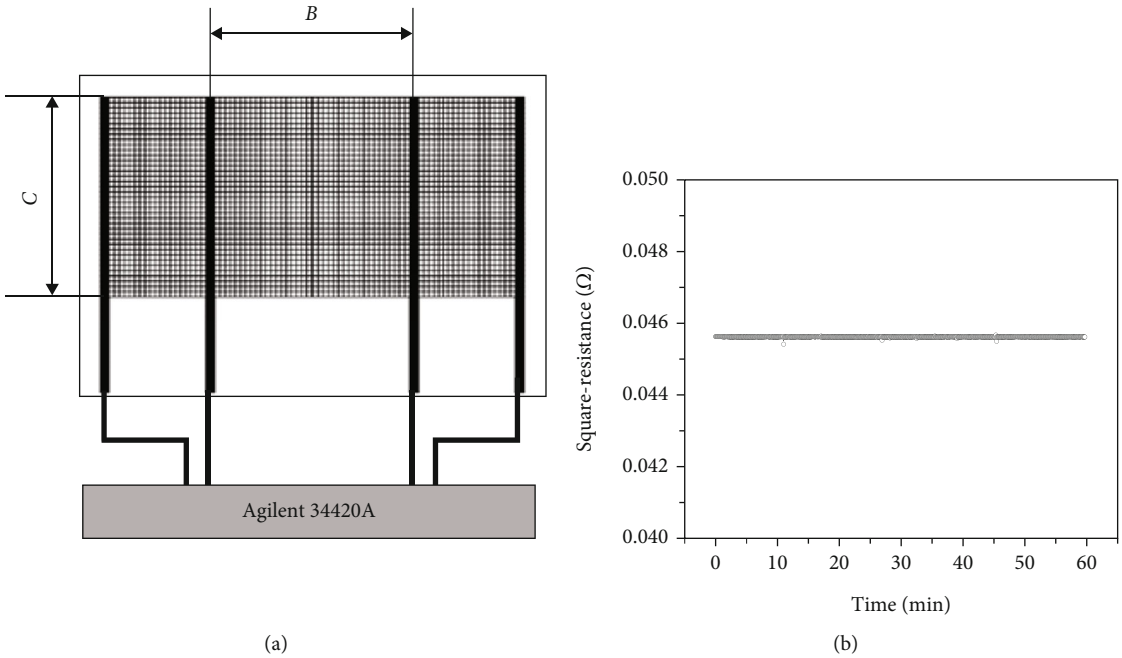

FIGURE 7: (a) Schematic diagram for measuring square resistance. (b) The measured results of the square resistance of the LMMF.

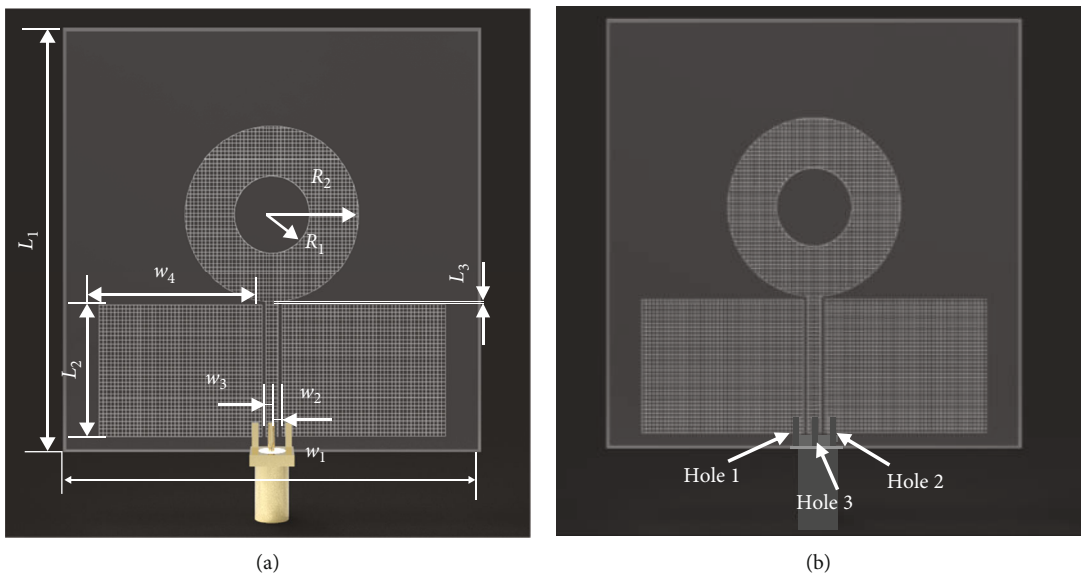

FIGURE 8: (a) Schematic diagram of the structure of a coplanar waveguide loop antenna. (b) Holes were punched in the antenna to install the SMA connector.

The resistivity of EGaIn is $\rho = 2.89 \times 10^{-7}\ \Omega$·m [33]. The case for $s = 500\ \mu$m, $w = 50\ \mu$m, and $H = 50\ \mu$m is selected as an example. Substituting these data into (5), the square resistance R of the LMMF is thus calculated as 0.063 Ω/sq.

For verification, the square resistance R of LMMF was measured using the four-wire method. The schematic diagram of the square resistance measurement is shown in Figure 7(a). The resistance R_m was measured and recorded with an Agilent 34420A nanoVolt/micro-Ohm meter. As can be seen in Figure 7(a), the bold black lines are four EGaIn-made electrodes to reduce contact resistance between the LM electrodes and the LM grid wire. According to the measurement principle of the four-wire method, the relationship between the square resistance R and the measured resistance R_m is as follows.

$$R = R_m \frac{C}{B}. \tag{6}$$

The parameters of the LMMF, including the line spacing

Table 1: Dimensions of the antenna (unit : mm).

Symbols	Values	Symbols	Values	Symbols	Values
W_1	60	W_2	0.5	W_3	2.0
W_4	23.5	L_1	60	L_2	18.7
L_3	0.54	R_1	5.5	R_2	12.6
T_1	1.0	T_2	1.0	H	0.05
s	0.5	w	0.05		

s, the width w, and the height H, are the same as those of the above calculation case. Both dimensions of C and D are 21 mm. Therefore, the measured resistance R_m is equal to the square resistance R. As shown in Figure 7(b), R_m was recorded for one hour and remained stable at approximately 0.0456 Ω/sq. Considering the very complex series-parallel problem involved in LMMF, there is an acceptable difference between the measured square resistance (0.0456 Ω/sq) and the calculated value (0.063 Ω/sq). In addition to the influence of the simplified calculation model, the precision of the fabrication of the liquid metal mesh is also an important factor.

3. Transparent Antenna Based on LMMF

3.1. Antenna Design and Fabrication. Figure 8(a) shows the structural diagram of the LMMF-based coplanar waveguide loop antenna. This antenna is fed by coplanar waveguide technology. There is a liquid metal mesh feed line in the center of the lower part of the PDMS, an annular radiator made of liquid metal mesh connected to the feeder, and two conductor planes made of symmetric liquid metal mesh on both sides of the feeder. Since the central feeder, the two conductor planes, and the annular radiator are all located on the same plane, only one bonding and one injecting are required in the fabrication of the LMMF-based transparent antenna. This shows that this structural design makes the processing very convenient. This antenna structure is referenced from previous studies [1], and all geometric dimensions of the antenna are optimized and listed in Table 1.

An SMA connector is connected to the feeder and two conductor planes to feed the transparent antenna. The positions of the three connecting holes on the LMMF are indicated in Figure 8(b). The three holes corresponded to the pin positions of the SMA connector as follows: holes 1 and 2 corresponded to the outer conductors of the SMA connector, and hole 3 corresponded to the inner conductor of the SMA connector.

The process for fabricating the antenna is as follows. First, according to the process described above, the PDMS bilayer film was prepared with grid flow channels as shown in Figure 8(a), and three holes were punched in the PDMS film as shown in Figure 8(b). Next, EGaIn droplets were dropped into the three holes, and the PDMS bilayer film containing EGaIn droplets was placed in the vacuum chamber and vacuumed to 10^{-4} Pa.

After the pressure has returned to atmospheric pressure, EGaIn is automatically filled into all flow channels. Then, the three pins of the SMA connector are inserted into the three holes accordingly. Subsequently, an appropriate amount of EGaIn is added into the three holes, ensuring good electrical contacts between the lead pins of the SMA connector, the feeder, and the coplanar waveguide. Finally, the contact

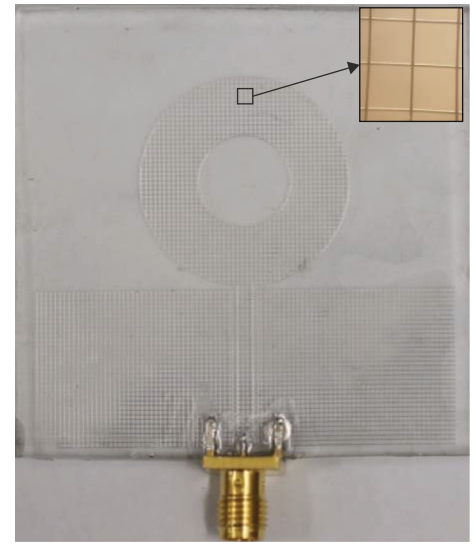

Figure 9: Photo of the highly transparent flexible antenna manufactured. The illustration in the upper right corner shows the grid wire of LM observed with an optical microscope.

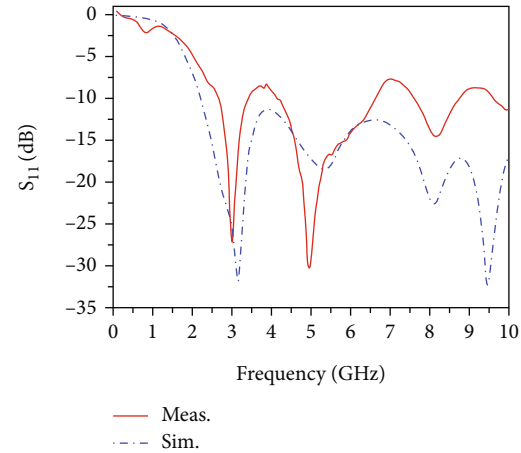

Figure 10: The measured and simulated reflection coefficients of the antenna.

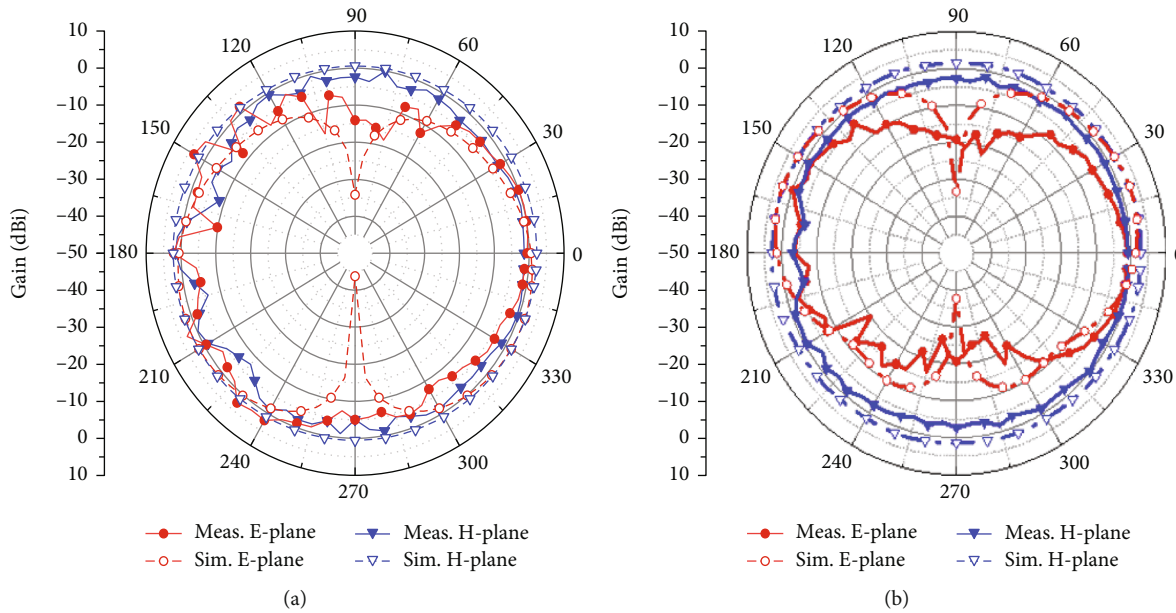

FIGURE 11: (a) The measured and simulated radiation patterns of the antenna in the E-plane and H-plane, at 3 GHz. (b) The measured and simulated radiation patterns of the antenna in the E-plane and H-plane, at 5 GHz.

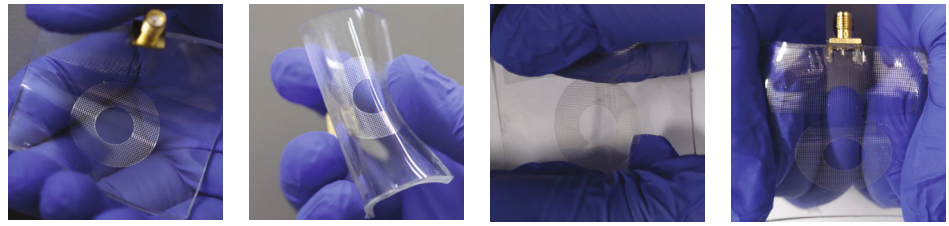

FIGURE 12: Repeated bending and stretching tests. (a) The antenna was bent forward. (b) The antenna was bent in the opposite direction. (c) The antenna was stretched in the front-back direction. (d) The antenna was stretched in the left-right direction.

surfaces between the SMA connector and the three holes are sealed with glue. A sample of the highly transparent flexible coplanar waveguide loop antenna, fabricated according to the above process, is shown in Figure 9.

3.2. Results and Discussion. A vector network analyzer (5063A, Keysight Technologies) was used to measure the *S* parameters of the antenna, and S_{11} was used to characterize the size of the antenna reflection coefficient. As shown in Figure 10, the reflection coefficient of the antenna varies with frequency. The simulation results indicate that the antenna is a low-reflection broadband antenna. In the range of 2.17-10 GHz, the S_{11} of the antenna is below -10 dB and presents multiple valleys at 3.17 GHz (-32 dB), 5.36 GHz (-18.5 dB), 8.11 GHz (-22.6 dB), and 9.48 GHz (-32.3 dB). The measurement results show that the S_{11} of the antenna is below -10 dB in four discrete ranges of 2.59-3.39 GHz, 4.14-6.58 GHz, 7.58-8.68 GHz, and 9.57-10.0 GHz. The corresponding multiple valley values occur at 2.99 GHz (-27.3 dB), 4.97 GHz (-30.3 dB), 8.08 GHz (-14.5 dB), and 9.88 GHz (-11.4 dB). Compared to the simulation results, the curve of the measurement results shifts upward at frequencies above 6.3 GHz, indicating that the reflection coefficient becomes larger, leading to some discontinuities in the continuous bandwidth with low reflections. The increase of the reflection coefficient and the shift of the resonant frequency in the measured results are acceptable, which may be caused by the accuracy of the antenna fabrication and measurement errors.

The antenna gain is measured at different frequencies and angles using a microwave darkroom (Institute of Antenna and Microwave Research, Tsinghua University), and then, the directionality coefficient and efficiency of the antenna are calculated. Figure 11 shows the measured and simulated radiation patterns of the E-plane and the H-plane when the antenna works at 3 GHz and 5 GHz, respectively. The radiation patterns show the shape of "8" on the E-plane and "O" on the H-plane. The simulated peak gains are 2.23 dBi (3 GHz) and 2.95 dBi (5 GHz), and the measured peak gains are 3.38 dBi (3 GHz) and -0.34 dBi (5 GHz), respectively. In addition, the average efficiencies of the simulation are all higher than 90%, while the average efficiencies of the measurement are 61% (3 GHz) and 43% (5 GHz), respectively. The errors in the measured gain and efficiency related to the simulation results are caused not only by the antenna manufacturing process and measurement errors but also by the offset of the main frequency.

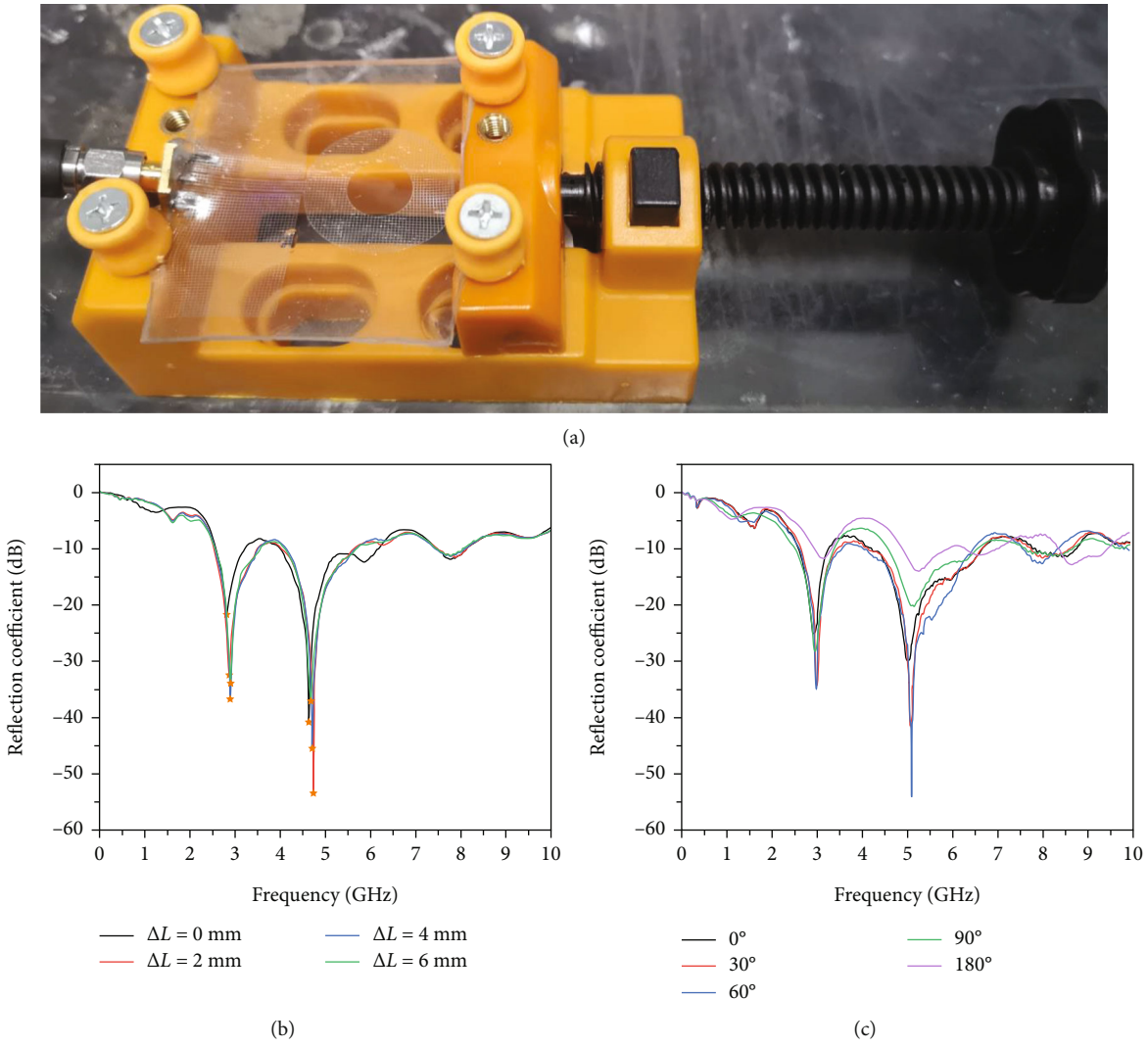

Figure 13: Reflection coefficient tests when the antenna is stretched and bent. (a) Fixture for fixing and stretching when measuring antenna reflection coefficients. (b) Reflection coefficient when the antenna is stretched. (c) Reflection coefficient when the antenna is bent.

Table 2: Comparison of transparent antennas with previous works.

Ref.	Conductive material	Substrate material	$L \times W$ (mm^2)	T (%)	R (Ω/sq)	Peak gain (dBi)	Measured average efficiency
[1]	ITO	Glass	50 × 50	57	5	0.5	75%
[2]	IZTO/Ag/IZTO	Polyimide	46 × 30	86	7.0189	1.84	53%
[3]	ITO/Ag/ITO	Glass	35 × 36.6	88	3.1	N/A	66%
[4]	Nano-structure thin film	Glass	200 × 150	80	5	1.28	66.52%
[5]	Conductive fabric tissue	PDMS	50 × 40	70	0.089	4.5	75%
[6]	IZTO/ag/IZTO	Acryl	50 × 50	68.6	2.52	-4.23	7.76%
[6]	Metal mesh film	Acryl	50 × 50	60	0.18	2.63	42.69%
[7]	Metal mesh film	Acryl	169 × 105	72	0.04	7.1	83.8%
This work	LMMF (EGaIn)	PDMS	60 × 60	72	0.0456	3.38	61%

As shown in Figure 12, the appearance of the antenna did not change after repeated bending and stretching. Additionally, after the above bending and stretching, there was almost no change in the S parameters, indicating that the antenna had not been damaged, as shown in Figure 13. Unlike solid metals and conductive oxides such as ITO and FTO, the conductive materials of LM would not affect the stretchable deformation ability of the antenna at all. In other words, the

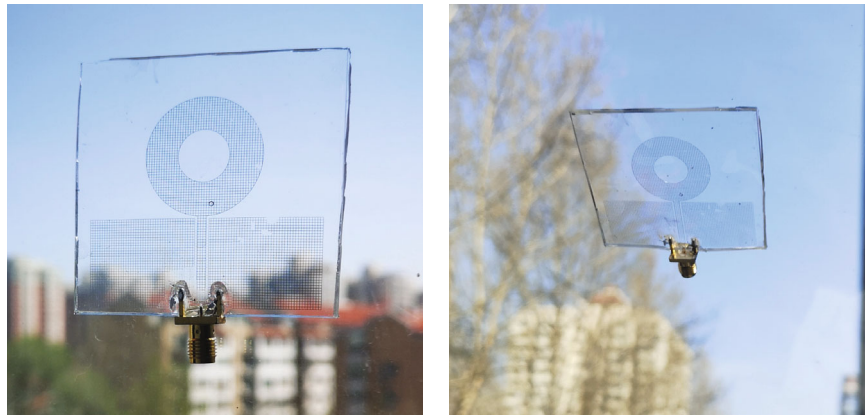

(a) (b)

FIGURE 14: The image of the highly transparent antennas was placed on the indoor glass and the car window glass. (a) The antenna was placed on the indoor window glass. (b) The antenna was placed on the car window glass.

flexibility and stretchability of the antenna depend on the substrate. PDMS has good stretchability and bendability, so the LMMF can recover spontaneously after stretching and bending within the elastic strain range of the PDMS. Additionally, improving the flexibility of the substrate can further improve the flexibility of the LM-based antenna.

3.3. Performance Comparison. Table 2 presents a comparison of the performance of this work and several transparent antennas disclosed in the published literature. First, when analyzing the transmittance and the square resistance, both do not perform well in [1]. The square resistance is too large (more than 3 Ω/sq), although the transmittance is better in [2–4] work; while the square resistance is lower in [5, 6], the transmittance is also too lower. In contrast, the square resistance and transmittance measured by the antenna in this paper are 0.0465 Ω/sq and 72%, respectively. Square resistance and transmittance are better than those of [5, 6]. The flexibility and stretchability of the antenna are then analyzed. In [7], copper mesh and acrylic were employed so that the antenna was completely inelastic. Several other works were also limited to solid conductive materials or substrates, such as ITO and glass, so the antennas were difficult to bend and stretch. In contrast, the antenna in this work and in [5] performs best from the point of view of flexibility. However, in [5], although PDMS was used as the substrate, it could not be stretched because of the conductive fibers. In this paper, as an application example of LMMF, the antenna used EGaIn (fluidic) as the conductive material and PDMS (flexible and stretchable) as the substrate, so the antenna could be easily bent and stretched.

In summary, taking the new material and process proposed in this paper, the proposed antenna in this work has a rare balance of conductivity, light transmission, and flexibility of the antenna. At the same time, the performance of the antenna in terms of impedance bandwidth, gain, and efficiency has reached a practical level. In the future, we will further optimize the antenna to obtain better gain and efficiency. In addition, the main factors that affect the square resistance are the width, spacing, and height of the EGaIn line. It can take measures to increase the line spacing and reduce the line width to further improve its transmittance; it can also increase the line height to reduce the square resistance of the antenna without reducing the transmittance. The flexibility and transmittance of the antenna can be improved by selecting an appropriate substrate. These conclusions point to the direction for further improvements in antenna conductivity, light transmittance, and flexibility.

3.4. Discussion on the Application of Antenna. Figure 14 shows the effect of placing the highly transmissive, flexible, stretchable, and reconfigurable antenna obtained in this paper on interior glass (flat glass) and car window glass (curved glass). The antenna on the glass does not have a significant visual impact, and it is easy to achieve a conformal fit on the curved surface. Of course, at present, it is inevitable that the SMA connector has some obstruction to the view. Its effect can be reduced by placing the SMA connector on a part other than the glass or by reducing the size of the connector. Even transparent connectors can be developed in the future. As we can see, this highly translucent, flexible, and stretchable antenna is suitable for applications that require stretching deformation or curved conformal capability. The materials and processes used in this paper can be applied to flexible antennas, stretchable antennas, conformal antennas, hidden antennas, aesthetic antennas, wearable electronics, or other RF electronic devices. The simulation results of the antenna show that the S_{11} of the antenna is below -10 dB in the range of 2.17-10 GHz. Although the measured results show some deviation, they also cover most of the S-band, C-band, and X-band, as well as multiple 5G communication. Therefore, the antenna can be used in fields such as radar and mobile communication.

Currently, we are already working on the development of antennas with multilayer liquid metal mesh films based on the work in this paper. In the future, we will further develop waveguide, phase shifter, and other microwave devices based on liquid metal grid films to achieve transparent and stretchable radio frequency electronics.

4. Conclusions

In this paper, the LMMF fabrication process and the corresponding antenna based on the LMMF are proposed. According to this process, a series of LMMFs with different line widths and line spacings is fabricated, and then, the light transmittance and square resistance of LMMF are theoretically and experimentally studied. To balance transmittance and square resistance, the line width and line spacing are set at 50 μm and 500 μm, respectively. For this case, the light transmittance is 72%, while the square resistance is 0.0456 Ω/sq. Thus, a highly transparent flexible coplanar waveguide loop antenna is designed and fabricated to verify the practicability of LMMF. The measured peak gain and average antenna efficiency are 3.38 dBi and 61% at 3 GHz, respectively. The antenna's operating frequencies cover most of the S-band, C-band, and X-band, as well as multiple channels for 5G communications. Therefore, the antenna can be used in areas such as radar and mobile communications. Overall, the fabrication of transparent antennas based on liquid metal mesh films is reported for the first time, and the antenna has good performance in light transmittance, square resistance, and flexibility at the same time. It implies important application prospects in transparent electronics, flexible electronics, and wearable electronics.

Data Availability

The data are available on request from the authors.

Conflicts of Interest

The authors declare that they have no known competing financial interests or personal relationships that could have appeared to influence the work reported in this paper.

Authors' Contributions

Peng Qin conducted the conceptualization, methodology, software, validation, formal analysis, investigation, resources, data curation, writing of the original draft preparation, writing the review and editing, and visualization; Qianyu Wang conducted the conceptualization, methodology, software, validation, investigation, resources, data curation, writing of the original draft preparation, writing the review and editing, and visualization; Pan Zhang was responsible for the software and validation; Guan-Long Huang conducted the writing of review and editing, and visualization; Qian Li conducted the validation and resources; Bingxin Liu was responsible of the software and resources; Lei Li was responsible for the resources and supervision; Lin Gui and Jing Liu managed the project administration and funding acquisition; Zhongshan Deng managed the conceptualization, supervision, project administration, and funding acquisition. All authors have read and agreed to the published version of the manuscript. Peng Qin and Qianyu Wang contributed equally to this research and should be regarded as co-first authors.

Acknowledgments

This work is supported by the National Key Research and Development Program of China (2019YFB2204903).

References

[1] M. R. Haraty, M. Naser-Moghadasi, A. A. Lotfi-Neyestanak, and A. Nikfarjam, "Improving the efficiency of transparent antenna using gold nanolayer deposition," *IEEE Antennas and Wireless Propagation Letters*, vol. 15, pp. 4–7, 2016.

[2] Y. Kim, C. Lee, S. Hong, C. W. Jung, and Y. Kim, "Design of transparent multilayer film antenna for wireless communication," *Electronics Letters*, vol. 51, no. 1, pp. 12–14, 2015.

[3] J. W. Kim, J. I. Oh, K. S. Kim, J. W. Yu, K. J. Jung, and I. N. Cho, "Efficiency-improved UWB transparent antennas using ITO/Ag/ITO multilayer electrode films," *IEEE Access*, vol. 9, pp. 165385–165393, 2021.

[4] S. C. Chiou, Y. M. Lin, T. C. Tai et al., "High efficiency transparent digital television antenna based on nano-structured thin film coating technology," in *2017 International Conference on Applied System Innovation (ICASI)*, pp. 500–502, Sapporo, Japan, May 2017.

[5] H. A. Elmobarak Elobaid, S. K. Abdul Rahim, M. Himdi, X. Castel, and K. M. Abedian, "A transparent and flexible polymer-fabric tissue UWB antenna for future wireless networks," *IEEE Antennas and Wireless Propagation Letters*, vol. 16, pp. 1333–1336, 2017.

[6] S. Hong, Y. Kim, and C. W. Jung, "Transparent microstrip patch antennas with multilayer and metal-mesh films," *IEEE Antennas and Wireless Propagation Letters*, vol. 16, pp. 772–775, 2017.

[7] P. D. Tung and C. W. Jung, "Optically transparent wideband dipole and patch external antennas using metal mesh for UHD TV applications," *IEEE Transactions on Antennas and Propagation*, vol. 68, no. 3, pp. 1907–1917, 2020.

[8] T. A. Elwi, "Printed microwave metamaterial-antenna circuitries on nickel oxide polymerized palm fiber substrates," *Nature Scientific Reports*, vol. 9, p. 2174, 2019.

[9] T. A. Elwi, "A further realization of a flexible metamaterial-based antenna on nickel oxide polymerized palm fiber substrates for RF energy harvesting," *Wireless Personal Communications*, vol. 115, no. 2, pp. 1623–1634, 2020.

[10] T. A. Elwi and A. M. Al-Saegh, "Further realization of a flexible metamaterial-based antenna on indium nickel oxide polymerized palm fiber substrates for RF energy harvesting," *International Journal of Microwave and Wireless Technologies*, vol. 13, no. 1, pp. 67–75, 2021.

[11] M. N. N. Alaukally, T. A. Elwi, and D. C. Atilla, "Miniaturized flexible metamaterial antenna of circularly polarized high gain-bandwidth product for radio frequency energy harvesting," *International Journal of Communication Systems*, vol. 35, article e5024, 2021.

[12] N. Guan, F. Hirotaka, D. Delaune, and K. Ito, "Radiation efficiency of monopole antenna made of a transparent conductive film," in *2007 IEEE Antennas and Propagation Society International Symposium*, pp. 221–224, Honolulu, HI, USA, June 2007.

[13] G. Sun, B. Muneer, and Q. Zhu, "A study of microstrip antenna made of transparent ITO films," in *2014 IEEE Antennas and Propagation Society International Symposium (APSURSI)*, pp. 1867-1868, Memphis, TN, USA, July 2014.

[14] T. A. Elwi, D. A. Jassim, and H. H. Mohammed, "Novel miniaturized folded UWB microstrip antenna-based metamaterial for RF energy harvesting," *International Journal of Communication Systems*, vol. 33, no. 6, article e4305, 2020.

[15] A. Al-Adhami and E. Erçelebi, "A reconfigurable flexible fractal-based monopole antenna for portable applications," *International Journal of Communication Systems*, vol. 34, article e4851, 2021.

[16] A. Al-Adhami and E. Ercelebi, "A flexible metamaterial based printed antenna for wearable biomedical applications," *Sensors*, vol. 21, no. 23, p. 7960, 2021.

[17] S. Hong, S. H. Kang, Y. Kim, and C. W. Jung, "Transparent and flexible antenna for wearable glasses applications," *IEEE Transactions on Antennas and Propagation*, vol. 64, no. 7, pp. 2797–2804, 2016.

[18] N. A. Eltresy, A. E. M. A. Elhamid, D. M. Elsheakh, H. M. Elhennawy, and E. A. Abdallah, "Silver sandwiched ITO based transparent antenna array for RF energy harvesting in 5G mid-range of frequencies," *IEEE Access*, vol. 9, pp. 49476–49486, 2021.

[19] N. A. Eltresy, A. M. Abd Elhamid, D. N. Elsheakh, E. A. Abdallah, and H. M. Elhennawy, "AgITO for high-performance semi-transparent wideband antenna applications," *Electronics Letters*, vol. 56, no. 15, pp. 749-750, 2020.

[20] A. Desai, T. Upadhyaya, J. Patel, R. Patel, and M. Palandoken, "Flexible CPW fed transparent antenna for WLAN and sub-6 GHz 5G applications," *Microwave and Optical Technology Letters*, vol. 62, no. 5, pp. 2090–2103, 2020.

[21] T. Peter, R. Nilavalan, H. F. AbuTarboush, and S. W. Cheung, "A novel technique and soldering method to improve performance of transparent polymer antennas," *IEEE Antennas and Wireless Propagation Letters*, vol. 9, pp. 918–921, 2010.

[22] D. Potti, G. N. A. Mohammed, K. Savarimuthu, S. Narendhiran, and G. Rajamanickam, "An ultra-wideband rectenna using optically transparent Vivaldi antenna for radio frequency energy harvesting," *International Journal of RF and Microwave Computer-Aided Engineeging*, vol. 30, article e22362, 2020.

[23] D. Potti, Y. Tusharika, M. G. Alsath et al., "A novel optically transparent UWB antenna for automotive MIMO communications," *IEEE Transactions on Antennas and Propagation*, vol. 69, no. 7, pp. 3821–3828, 2021.

[24] J. H. Fu, C. L. Zhang, T. Y. Liu, and J. Liu, "Room temperature liquid metal: its melting point, dominating mechanism and applications," *Frontiers in Energy*, vol. 14, no. 1, pp. 81–104, 2020.

[25] D. M. Hensley, C. G. Christodoulou, and N. Jackson, "A stretchable liquid metal coaxial phase shifter," *IEEE Open Journal of Antennas and Propagation*, vol. 2, pp. 370–374, 2021.

[26] K. Y. Chan, R. Ramer, and R. Sorrentino, "Low-cost Ku-band waveguide devices using 3-D printing and liquid metal filling," *IEEE Transactions on Microwave Theory and Techniques*, vol. 66, no. 9, pp. 3993–4001, 2018.

[27] P. Qin, L. Wang, T. Y. Liu et al., "The design and manufacturing process of an electrolyte-free liquid metal frequency-reconfigurable antenna," *Sensors*, vol. 21, no. 5, p. 1793, 2021.

[28] K. N. Paracha, A. D. Butt, A. S. Alghamdi, S. A. Babale, and P. J. Soh, "Liquid metal antennas: materials, fabrication and applications," *Sensors*, vol. 20, no. 1, p. 177, 2020.

[29] P. Qin, G. L. Huang, J. J. Liang et al., "A gravity-triggered liquid metal patch antenna with reconfigurable frequency," *Micromachines*, vol. 12, no. 6, p. 701, 2021.

[30] C. F. Pan, K. Kumar, J. Z. Li, E. J. Markvicka, P. R. Herman, and C. Majidi, "Visually imperceptible liquid-metal circuits for transparent, stretchable electronics with direct laser writing," *Advanced Materials*, vol. 30, no. 12, article 1706937, 2018.

[31] L. Dejace, H. T. Chen, I. Furfaro, G. Schiavone, and S. P. Lacour, "Microscale liquid metal conductors for stretchable and transparent electronics," *Advanced Materials Technologies*, vol. 6, no. 11, p. 2100690, 2021.

[32] P. D. Tung and C. W. Jung, "High optical visibility and shielding effectiveness metal mesh film for microwave oven application," *IEEE Transactions on Electromagnetic Compatibility*, vol. 62, no. 4, pp. 1076–1081, 2020.

[33] Q. X. Liang, Z. Yang, J. Y. Guo, Z. H. Li, T. N. Chen, and D. C. Li, "A high-efficient tunable liquid metal-based electromagnetic absorbing metamaterial," *Journal of Materials Science: Materials in Electronics*, vol. 31, no. 21, pp. 19242–19247, 2020.